The Mindanao and Halmahera Eddies—Twin Eddies Induced by Nonlinearities

WILTON Z. ARRUDA* AND DORON NOF+

Department of Oceanography, The Florida State University, Tallahassee, Florida

(Manuscript received 27 June 2002, in final form 8 May 2003)

ABSTRACT

It is shown analytically that a nonlinear collision of northward- and southward-flowing western boundary currents (WBC) on a β plane produces both an anticyclonic and a cyclonic eddy. (On an f plane no eddies are established; similarly, no eddies are established in the linear limit.) The length scales of both the anticyclonic and cyclonic eddies are larger than most eddies in the ocean. Furthermore, the anticyclone scale is larger than the cyclone length scale because of the higher upstream momentum flux. A reduced-gravity numerical model is used to validate these analytical results. The balance of forces and the eddy size estimates (derived from the numerical simulations) agree with the analytical results. Based on the above collision problem, it is argued that the Halmahera and Mindanao eddies are required to balance the nonlinear momentum fluxes of their colliding parent currents, the southward-flowing Mindanao Current (MC) and the northward-flowing South Equatorial Current (SEC). Assuming that the interior is in Sverdrup balance, it is further argued that neither of the eddies would have been present had the Indonesian Throughflow not been active.

1. Introduction

The western equatorial Pacific plays a key role in the establishment of El Niño–Southern Oscillation (ENSO) events and may also be an important part of the so-called ''great conveyor belt'' (e.g., Gordon 1986) because of the Pacific-to-Indian throughflow. The eddies and low-latitude western boundary currents (WBC) addressed here (Fig. 1) are important aspects of these processes.

The equatorward-flowing WBCs provide the closure to two symmetrical gyres relative to the equator (Kessler and Taft 1987). One gyre is entirely in the Northern Hemisphere whereas the other (which is mostly in the Southern Hemisphere) crosses the equator. The North Equatorial Countercurrent (NECC) forms the boundary between these two gyres at about 5°N. North of the NECC the westward-flowing North Equatorial Current (NEC) bifurcates (Toole et al. 1990) into the northward-flowing Kuroshio and the southward-flowing Mindanao Current (MC). A similar situation takes place in the Southern Hemisphere where the westward-flowing South Equatorial Current (SEC) bifurcates (around 15°S) into a branch flowing northwestward and a branch flowing southward. Along the New Guinea coast the northwestward-flowing branch of the SEC is usually recognized as a subsurface current, the New Guinea Coastal Undercurrent (NGCUC), and a surface current, the New Guinea Coastal Current (NGCC). The NGCC retroflects to the east of the Halmahera Island and joins the retroflected flow of the MC to flow eastward as the NECC.

There are two semipermanent eddies in the retroflection area of the MC and SEC (Fig. 1). The first, the Mindanao eddy (ME), is situated north of the NECC (near 7°N, 128°E) and has cyclonic circulation, whereas the second, the Halmahera eddy (HE), which is situated south of the NECC (near 4°N, 130°E), has anticyclonic circulation (Wyrtki 1961). The reason for the existence of the eddies is not obvious. One would intuitively expect that such eddies are established by friction that enables the turning fluid to drag some interior fluid along with it as it turns. Another possibility would be that the eddies result from instability of the eastward flowing NECC and the westward propagation of such instabilities. We shall show in this article that neither of the two ideas is correct. We shall demonstrate that both friction and instability do not play any role in the establishment of the eddies. Rather, it is nonlinearity and β that are responsible for the establishment of the eddies. In what follows we shall briefly describe the two

* Permanent affiliation: Departamento de Métodos Matemáticos, Universidade Federal do Rio de Janeiro, Rio de Janeiro, Brazil.

+ Additional affiliation: Geophysical Fluid Dynamics Institute, The Florida State University, Tallahassee, Florida.

Corresponding author address: Prof. Doron Nof, Department of Oceanography 4320, The Florida State University, Tallahassee, FL 32306-4320.
E-mail: nof@ocean.fsu.edu

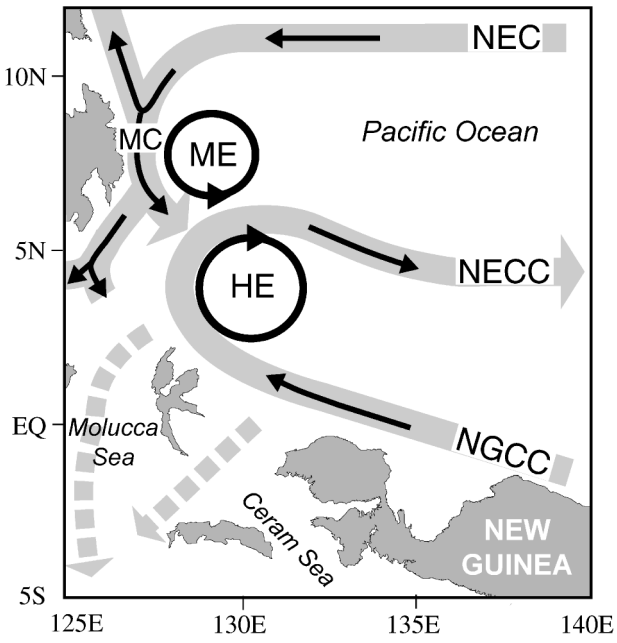

FIG. 1. The flow pattern in the western equatorial Pacific (adapted from Ffield and Gordon 1992). The Mindanao eddy and the Halmahera eddy are semipermanent and do not usually drift away from their generation area. Dashed arrows denote the southern part of the Indonesian Throughflow.

colliding boundary currents (MC and SEC) and the two eddies.

a. Observational background

1) THE MINDANAO CURRENT (MC)

The MC extends to a depth of 600 m and a distance of 100 km offshore (Wyrtki 1961; Masuzawa 1968). Wyrtki (1956, 1961) first estimated a baroclinic transport ranging from 8 to 12 Sv (Sv $\equiv 10^6$ m^3 s^{-1}) in the upper 200 m and 25 Sv in the upper 1000 m. Different transport estimates were later made by Masuzawa (1969) who gave a transport from 13 to 29 Sv relative to 600 dbar, Kendall (1969) who argued that the MC carries 14 Sv, Cannon (1970) who estimated a geostrophic transport of 18–31 Sv relative to 1000 dbar, Toole et al. (1988) who gave a transport of 17–18 Sv for waters warmer than 12°C, and Lukas et al. (1991) who calculated a transport from 13 to 33 Sv between 10° and 5.5°N. Regardless of the values that one chooses, the velocities are relatively high [O(1 m s^{-1})] and the width is fairly narrow (150 km). These give a fairly high Rossby number (~0.5 taking into account that the maximum speed is at that jet's center), suggesting that the current is nonlinear.

2) THE MINDANAO EDDY (ME)

Takahashi (1959) first noted the existence of ''a cold region of distorted elliptic form'' east of the MC and related this feature to the cyclonic circulation inferred from dynamic topography. This closed circulation is named the ''Mindanao eddy'' following the work of Wyrtki (1961) who noted that the ME is a quasi-permanent eddy associated with the turning of the NEC waters at the coast of the Philippines and its subsequent flow to the east as part of the NECC. The existence of the eddy was later verified by Lukas et al. (1991) who reported that drifters launched in the ME described closed loops with diameters of about 250 km and by Qu et al. (1999) who identified the ME as a depression (of less than 130 m) in the 24.5 σ_θ isopycnal surface centered at 7°N, 129°E.

3) THE SOUTH EQUATORIAL CURRENT AND THE NEW GUINEA COASTAL CURRENT

As mentioned, the westward-flowing SEC bifurcates near 15°S. The equatorward branch of the Great Barrier Reef Undercurrent (Church and Boland 1983) later flows into the NGCUC. A shallow current (NGCC) overlying the NGCUC was first observed by Masuzawa (1968). Cantos-Figuerola and Taft (1983) found a NGCC transport of 11 Sv, whereas Wyrtki and Kilonsky (1984) estimated a total transport (NGCC plus NGCUC) of about 40 Sv. Gouriou and Toole (1993) found a total transport of 24.8 Sv from direct measurements, 37.7 Sv from geostrophy relative to 600 dbar, and 41.7 Sv from geostrophy relative to 1000 dbar. Like the MC, the NGCC is fairly nonlinear, with a Rossby number of approximately 0.4.

4) THE HALMAHERA EDDY (HE)

As with the ME, the HE appears in the dynamics topography maps of Takahashi (1959) and was named after the work of Wyrtki (1961). It is well developed only during the northern summer monsoon, when the South Pacific water from the NGCC recurves into the NECC. Within the HE, Lukas et al.'s (1991) drifters executed closed loops of about 300 km diameter and velocity of about 50 cm s^{-1}. Using shipboard ADCP, Kashino et al. (1999) identified the center of the Halmahera eddy to be east of 130°E at 4°N. They also identified a horizontal scale of about 500 km (at 50 m).

b. Modeling and theoretical background

It is sufficient to point out here that there are no explanations for the establishment of the eddies, primarily because the earlier theories are linear (i.e., quasigeostrophic) which, as we shall see, filters out the eddy generation mechanism (Cessi 1990, 1991) or f-plane theories (Lebedev and Nof 1996, 1997), which also filters out the eddies.

Before proceeding, it is appropriate to point out that the Indonesian Throughflow (ITF) is critical to the collision of the MC and the NGCC and, therefore, to the

establishment of the eddies. Arruda (2002) showed that, without any net meridional flow a few degrees north of the equator (i.e., no ITF), there would be no WBC transport and, hence, no collision and no eddies. This is consistent with the picture described in Nof (1998) (see his Fig. 2) where, because of the vanishing wind stress curl a few degrees north of the equator (implying zero Sverdrup transport there) and the absence of deep water formation in the northern Pacific, there can be no WBC a few degrees north of the equator unless the basin has ''holes.'' Namely, with Sverdrup dynamics and zero wind stress curl north of the equator, a no-ITF scenario must involve no net WBC transport (i.e., no collision) because, in a closed basin, the WBC transport is equal and opposite to the interior transport (zero in our case).

c. Present work

As mentioned, our goal is to examine the nonlinear collision of opposing WBCs on a β plane. We shall see that it is the nonlinear curving of these retroflecting currents and β that are responsible for the generation of the eddies. Since our problem involves nonlinearity, a ''head-on'' approach is not useful, and we shall look at the problem in terms of integrated momentum flux balances that circumvent the need to find a solution valid in the entire field. Before attacking the full collision problem, it is useful to first examine the behavior of currents in a concave solid corner formed by a solid boundary. We shall do so by using the momentum flux approach (see, e.g., Lebedev and Nof 1996, 1997) and begin by examining a *northward*-flowing current.

This paper is organized as follows. After presenting the method of analysis in section 2, we address the problem of a WBC in a concave solid corner in section 3. In section 4 we focus on the collision problem, and in section 5 we apply the results of the previous sections to the equatorial western Pacific and suggest the physical mechanism responsible for the existence of the ME and HE. The conclusions are given in section 6.

2. Flow in a concave solid corner

a. Analytical considerations

1) FORMULATION

As the WBC (Fig. 2) flows northward, it encounters a zonal wall that forces it to change direction and flow eastward. Assuming a steady state and integrating (after multiplying by h) the steady and inviscid nonlinear y-momentum equation over the fixed region S bounded by the dashed line ABCDA (shown in the upper-left panel in Fig. 2), we get

$$\iint_S \left[\frac{\partial(huv)}{\partial x} + \frac{\partial(hv^2)}{\partial y}\right] dx\, dy - \iint_S f_0 \frac{\partial \psi}{\partial y}\, dx\, dy - \iint_S \left[\frac{\partial(\beta y \psi)}{\partial y} - \beta\psi\right] dx\, dy + \frac{g'}{2}\iint_S \frac{\partial(h^2)}{\partial y}\, dx\, dy = 0. \tag{1}$$

Application of Green's theorem gives

$$\oint_{\partial S} huv\, dy - \oint_{\partial S}\left[hv^2 + \frac{g'h^2}{2} - (f_0 + \beta y)\psi\right] dx + \beta\iint_S \psi\, dx\, dy = 0, \tag{2}$$

where ∂S is the boundary of S and g' is the reduced gravity, $g\Delta\rho/\rho$.

Next, we take $\psi = 0$ along the wall and note that at least one of the velocity components vanishes on every portion of the boundary ∂S. It then follows from (2) that

$$\int_A^B \left[hv^2 + \frac{g'h^2}{2} - (f_0 + \beta y)\psi\right] dx - \int_C^D \frac{g'h^2}{2}\, dx - \beta\iint_S \psi\, dx\, dy = 0. \tag{3}$$

Assuming now (and later verifying with our numerics) that, away from the corner, the flow is geostrophic in the cross-current direction, we get [after multiplying the geostrophic relation $(f_0 + \beta y)v = g'\partial h/\partial x$ by h and integration in x],

$$(f_0 + \beta_y)\psi = [h^2 - h(0, y_s)^2]. \tag{4}$$

Combining (3) and (4) we get our desired expression,

$$\underbrace{\int_0^L hv^2\, dx}_{\text{WBC momentum flux}} + \underbrace{\frac{g'}{2}\int_0^{L_2} [h^2(0, y_s) - h^2(x, 0)]\, dx}_{\text{pressure term}} \underbrace{- \beta\iint_S \psi\, dx\, dy}_{\beta\text{ term}} = 0, \tag{5}$$

where L is the boundary current width and L_2 is the zonal extent of our region S. It is straightforward to show that, for southward-flowing WBC, the equivalent momentum balance in the region S (bounded by ABCD) is very similar.

2) THE f-PLANE LIMIT

Although β is important for the establishment of the WBC in the first place, once a WBC is established, the role of β is frequently minor, particularly if the process in question is of the Rossby radius scale. For this reason, it makes sense to first examine the behavior of a boundary current on an f plane.

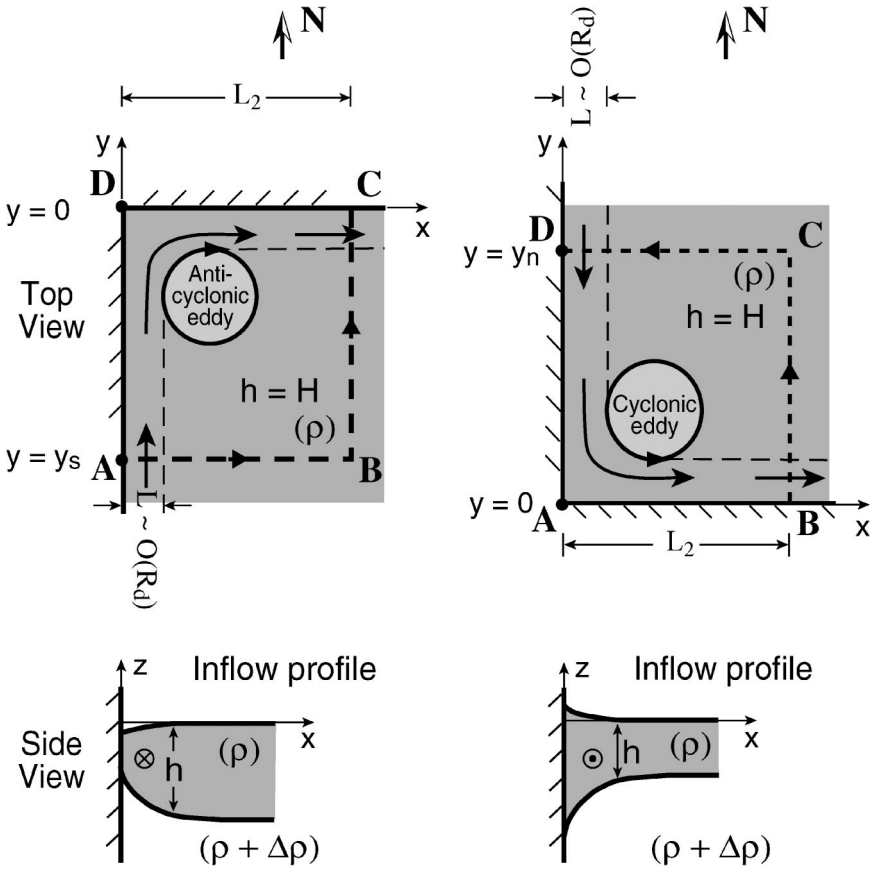

FIG. 2. Schematic diagram of the solid corner model. (upper) A northward- (southward-) flowing western boundary current encountering a zonal wall. Here H is the upper layer far east from the western boundary on a latitude a few Rossby radii away from the zonal wall. (lower) Vertical cross section of the approaching northward- (southward-) flowing WBC.

On an f plane the pressure force should balance the WBC momentum flux if a steady state is to be established. To see this, note that, as we approach the corner, the velocity along the wall gradually decreases to zero (see Kundu 1990, chapter 4). Since the wall is a streamline, the Bernoulli function [$B = g'h + (u^2 + v^2)/2$] implies that the upper-layer thickness increases to a maximum at the corner (Fig. 3, upper panel). Consequently, the pressure force in (5) points in the opposite direction to that of the WBC momentum force and a balance without an eddy appears to be possible. Numerical simulations will later verify this outcome. Note that, in the case of no zonal wall (i.e., the WBC separates due to a vanishing upper-layer thickness), the pressure term vanishes (since $h = 0$ on the western boundary and on the outcropping streamline). As a result, the WBC momentum flux is *unbalanced* and the f-plane system cannot reach a steady state (see Arruda et al. 2003, manuscript submitted to *Deep-Sea Res.*).

3) THE "NO EDDY ON A β PLANE" SCENARIO

Here, we temporarily assume that no eddy is associated with the turning boundary current on a β plane and show that this hypothetical scenario is impossible. Note that the geostrophic transport relationship [$T = g'(H^2 - h_w^2)/2f$, where H and h_w are the thicknesses off and on the wall] implies that on a β plane the near-wall thickness of a northward-flowing WBC decreases as we proceed downstream along the western boundary (Fig. 3, lower panel). This implies that there is an additional pressure force (resulting from the decreasing near-wall thickness due to β) pointing in the same sense as the upstream momentum flux. Hence, the wall pressure cannot balance the net (upstream) northward force. Taking the zonal extent of S to be $O(R_d)$ we see that, in the absence of an eddy, the β term in (5) is negligible when compared with the WBC momentum flux so that it cannot balance the WBC momentum flux either. The *no-eddy* scenario is, therefore, *impossible.* In what follows, we first present numerical simulations and then present our analytical solution.

b. Numerical simulation for a flow in a concave solid corner

We use a reduced-gravity version of the isopycnic model developed by Bleck and Boudra (1981, 1986)

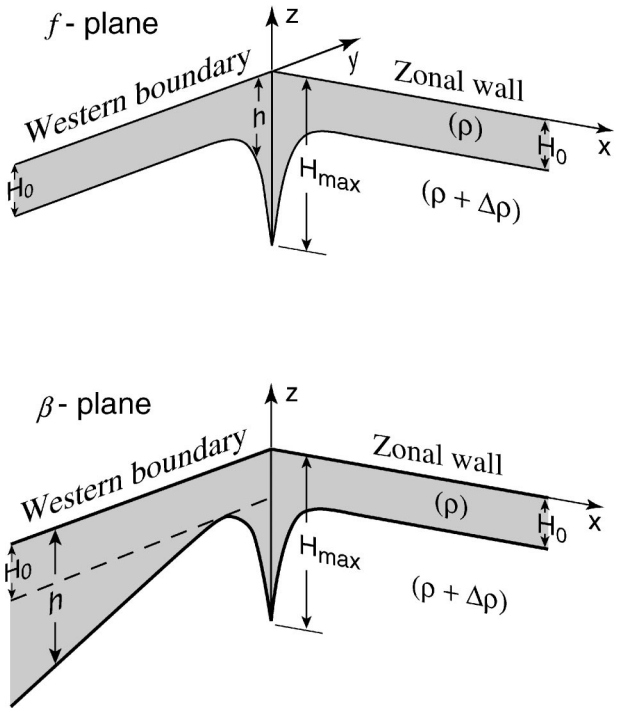

FIG. 3. Schematic three-dimensional diagram of the upper-layer thicknesses on the boundaries of a northward-flowing western boundary current (upper) on an f plane and (lower) on a β plane. Note that the upstream near-wall thickness is greater in the β-plane case. This is why the eddy is established (see text).

and later improved by Bleck and Smith (1990). The equations of motion are the two momentum equations,

$$\frac{\partial u}{\partial t} + u\frac{\partial u}{\partial x} + v\frac{\partial u}{\partial y} - (f_0 + \beta y)v = -g'\frac{\partial h}{\partial x} + \frac{\nu}{h}\nabla \cdot (h\nabla u) \quad \text{and}$$

$$\frac{\partial u}{\partial t} + u\frac{\partial v}{\partial x} + v\frac{\partial v}{\partial y} - (f_0 + \beta y)u = -g'\frac{\partial h}{\partial y} + \frac{\nu}{h}\nabla \cdot (h\nabla v), \tag{6}$$

and the continuity equation,

$$\frac{\partial h}{\partial t} + \frac{\partial (hu)}{\partial x} + \frac{\partial (hv)}{\partial y} = 0, \tag{7}$$

where ν is the frictional coefficient.

The model uses the Arakawa (1966) C grid where the u-velocity points are shifted one-half grid step to the left from h points, the v-velocity points are shifted one-half grid step down from the h points, and vorticity points are shifted one-half grid step down from the u-velocity points. On open boundaries the Orlanski (1976) second-order radiation boundary condition was implemented. The list of experiments is given in Table 1. The walls were slippery and the vorticity was taken to be zero near them.

TABLE 1. Table of experiments. The parameters $f_0 = 0.8573 \times 10^{-4}$ s^{-1}, $g' = 0.014$ m^2 s^{-1}, $\Delta x = \Delta y = 7.5$ km (horizontal resolution), and $\Delta t = 12$ min (time step) are common for all experiments.

Expt	Expt description	Parameters	Rossby radius (km)	Current transport	Shown in Fig.
E1	f-plane solid corner	$\beta = 0$, $\nu = 50$ m^2 s^{-1}, $H = 360$ m, $H_0 = 270.3$ m	$R_d = 26.2$	4.6 Sv (northward)	5, 6, 7
E2	f-plane solid corner	$\beta = 0$, $\nu = 50$ m^2 s^{-1}, $H = 200$ m, $H_0 = 270.3$ m	$R_d = 19.5$	2.6 Sv (southward)	8, 9, 10
E3	β-plane solid corner/ anticyclone	$\beta = 1.849 \times 10^{-11}$ m^2 s^{-1}, $\nu = 500$ m^2 s^{-1}, $H = 360$ m, $H_0 = 270.3$ m	$R_d = 26.2$	4.6 Sv (northward)	
E4	β-plane solid corner/ cyclone	$\beta = 1.849 \times 10^{-11}$ m^2 s^{-1}, $\nu = 500$ m^2 s^{-1}, $H = 200$ m, $H_0 = 270.3$ m	$R_d = 19.5$	2.6 Sv (southward)	
E5	β-plane solid corner/ anticyclone	$\beta = 1.849 \times 10^{-11}$ m^2 s^{-1}, $\nu = 1500$ m^2 s^{-1}, $H = 360$ m, $H_0 = 270.3$ m	$R_d = 26.2$	4.6 Sv (northward)	5, 6, 7
E6	β-plane solid corner/ cyclone	$\beta = 1.849 \times 10^{-11}$ m^2 s^{-1}, $\nu = 1500$ m^2 s^{-1}, $H = 200$ m, $H_0 = 270.3$ m	$R_d = 19.5$	2.6 Sv (southward)	8, 9, 10
E7	β-plane solid corner/ anticyclone	$\beta = 1.849 \times 10^{-11}$ m^2 s^{-1}, $\nu = 3000$ m^2 s^{-1}, $H = 360$ m, $H_0 = 270.3$ m	$R_d = 26.2$	4.6 Sv (northward)	
E8	β-plane solid corner/ cyclone	$\beta = 1.849 \times 10^{-11}$ m^2 s^{-1}, $\nu = 3000$ m^2 s^{-1}, $H = 200$ m, $H_0 = 270.3$ m	$R_d = 19.5$	2.6 Sv (southward)	
E9	β-plane collision	$\beta = 1.849 \times 10^{-11}$ m^2 s^{-1}, $\nu = 1500$ m^2 s^{-1}, $H = 200$ m, $H_0 = 270.3$ m	$R_{dn} = 19.5$ $R_{ds} = 26.2$	2.6 Sv (southward) 4.6 Sv (northward)	13, 14, 15

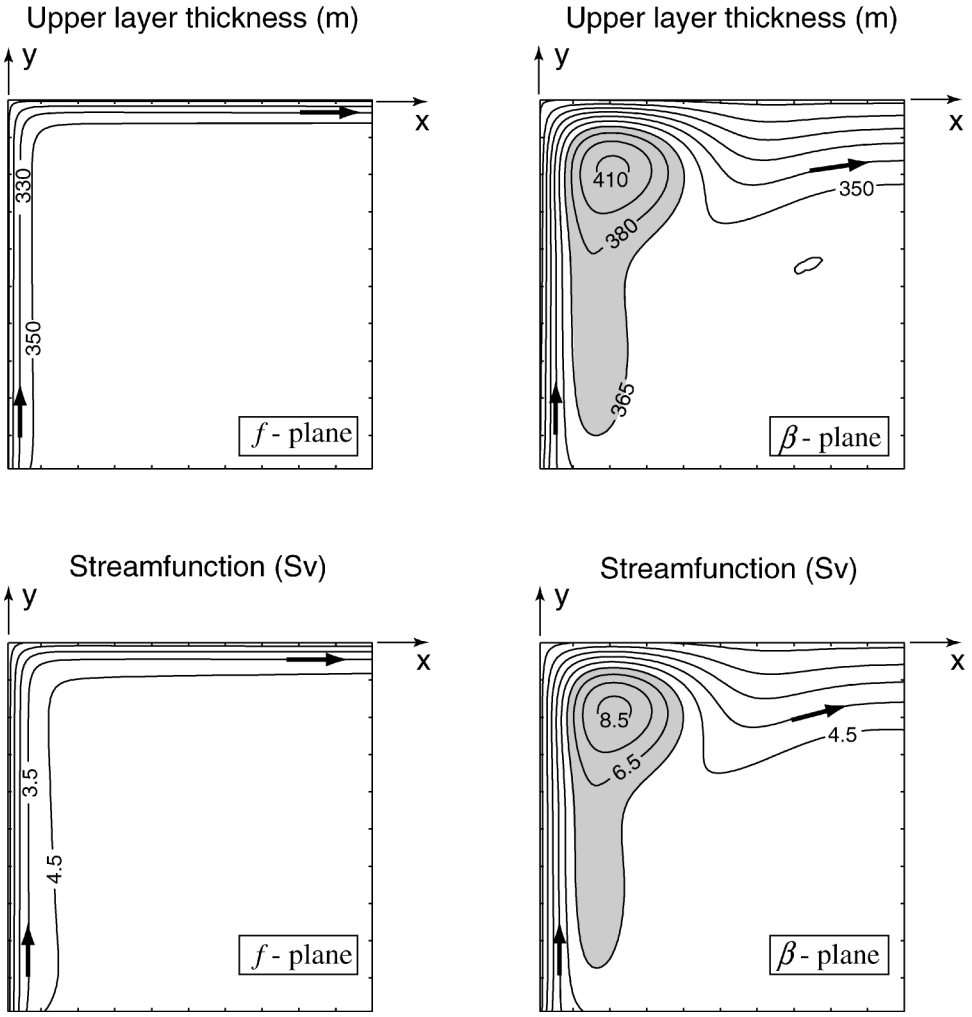

FIG. 4. (upper left) Upper-layer thickness contours and (lower left) streamfunction contours for the f-plane experiment E1 (Table 1) at day 2500; (upper right) upper-layer thickness contours and (lower right) streamfunction contours for the β-plane experiment E5 (Table 1) at day 2500. The contour spacing is 20 m for the upper-layer thickness and 15 Sv for the streamfunction. The axis marks are 10 grid points (75 km) apart. Areas within the closed contours are shaded.

1) NORTHWARD-FLOWING WBC IN A CONCAVE CORNER

Figure 4 shows the upper-layer thickness and streamfunction for the f-plane experiment E1 and the β-plane experiment E5 (Table 1) at day 2500, and Fig. 5 shows the upper-layer thickness along the western boundary and along the zonal wall. We see that, as mentioned, on an f plane the upper-layer thickness increases to a maximum near the corner, producing a southward pressure force. For the f-plane experiment E1 the downstream upper-layer thickness along the zonal wall is 270.7 m, which is very close to our specified value of 270.3 for H_0. Figure 6 shows that the pressure force points southward and balances the northward momentum flux of the WBC (indicating that the inviscid balance is attained). We also see that, as mentioned, in this f-plane case, no eddy is necessary to achieve the momentum balance.

When β is introduced (Fig. 4), an anticyclonic eddy (attached to the curving flow) is generated. As seen in Fig. 5, in this case, the net pressure force points northward since the upper-layer thickness along the western boundary is larger than its average value on the zonal wall (270.2 m). In addition, note that the thickening of the upper layer at the corner is compensated by the eddy so that the average value of the upper-layer thickness on the zonal wall is 270.2 m, which is practically indistinguishable from the initial value for H_0 (270.3 m). This numerical observation will be used shortly in our detailed derivations. Figure 6 shows that the combination of β and the pressure terms is a southward force that balances the northward momentum force of the WBC. With the aid of (5) and a scale analysis, which we shall perform later, we shall show that the eddy is the main contributor to the combined β and pressure

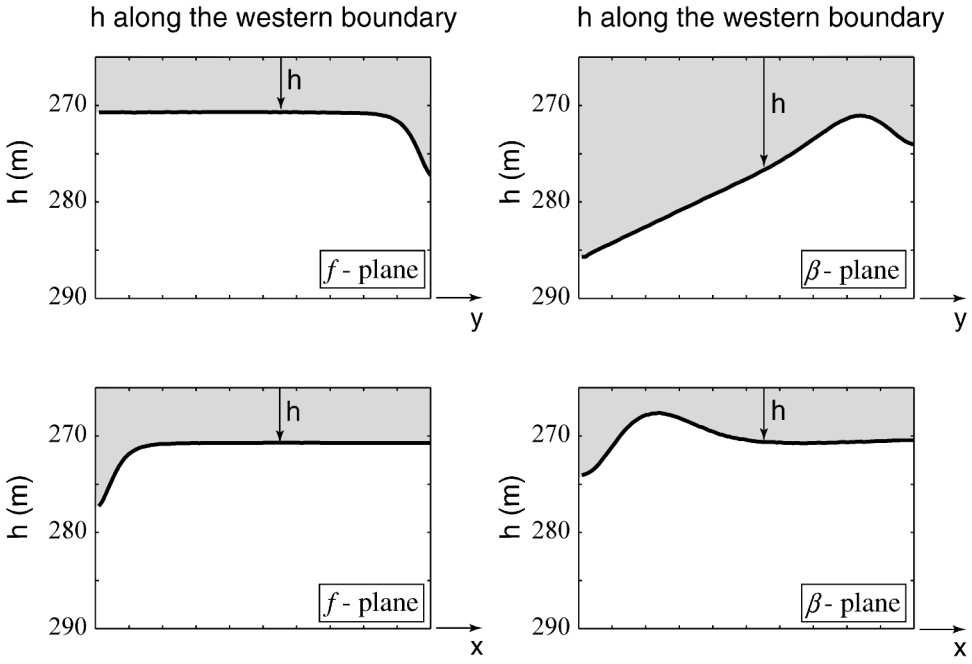

FIG. 5. The f-plane upper-layer thickness h (m) along the (upper left) western boundary and (lower left) along the zonal wall at day 2500; β-plane upper-layer thickness h (m) along the (upper right) western boundary and (lower right) zonal wall at day 2500. Shaded area is the upper layer. The horizontal axis marks are 10 grid points (75 km) apart.

terms. The eddy's β force is due to the particle circulation within the anticyclonic eddy that causes a greater Coriolis force on the northern portion of the eddy than on the southern.

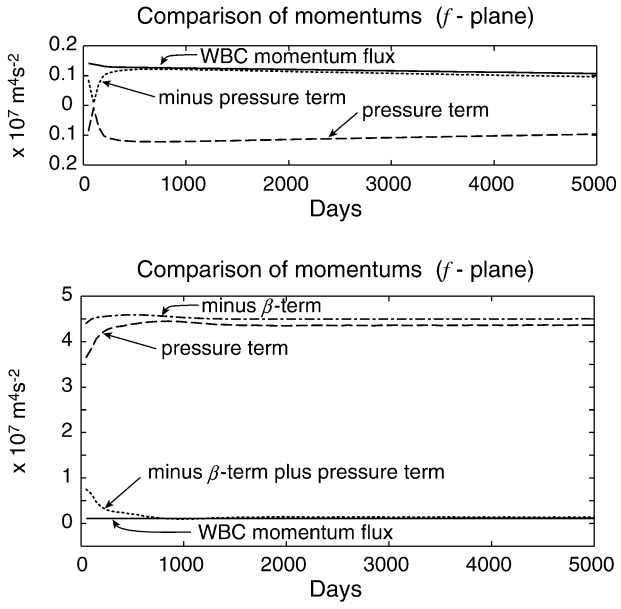

FIG. 6. Terms of the momentum balance (9) computed from (upper) the f-plane expt E1 and (lower) the β-plane expt E5. Note that, by day 500 for the f-plane run and day 800 for the β-plane run, the steady-state balance holds.

2) SOUTHWARD-FLOWING WBC IN A CORNER

Figure 7 shows contour plots of the upper-layer thickness and streamfunction at day 2500 for the f-plane experiment (E2) and the β-plane experiment (E6). Similarly, Fig. 8 displays the upper-layer thickness along the western boundary and along the zonal wall at the same day. In the f-plane situation, the upper-layer thickness increases to a maximum in the corner, producing a northward pressure force that, according to Fig. 9, balances the southward momentum force of the WBC. This indicates that the inviscid balance is attained.

When β is introduced (Fig. 7), a cyclonic eddy is formed. Also, as seen in Fig. 8, the pressure force points southward since the upper-layer thickness along the western boundary is larger than its average value on the zonal wall (268.6 m). The average value of the upper-layer thickness along the zonal wall is 268.6 m, which coincides with its average value at the last 50 grid points, showing that the thickening at the corner (associated with the Bernoulli function conservation) is compensated by the shallowness produced by the eddy. Again, this will shortly be used in our derivations. As seen in Fig. 9, the combination of the β and the pressure terms is a northward force that balances the southward momentum force of the WBC.

c. Estimates of the eddy radius

We shall now use both the analytical considerations given in section 3a and the numerical simulation given

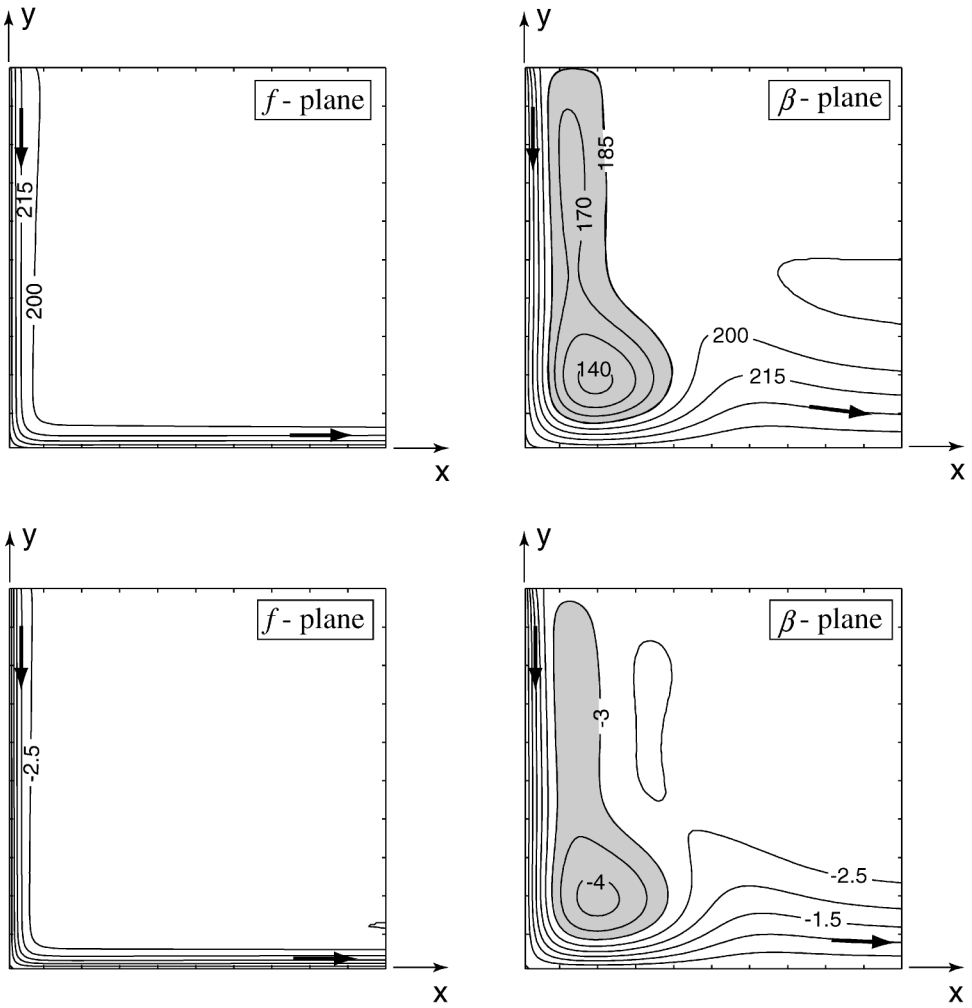

FIG. 7. (upper left) Upper-layer thickness contours and (lower left) streamfunction contours for the f-plane expt E2 (Table 1) at day 2500; (upper right) upper-layer thickness contours and (lower right) streamfunction contours for the β-plane expt E6 (Table 1) at day 2500. The contour spacing is 20 m for the upper-layer thickness and 15 Sv for the streamfunction. The axis marks are 10 grid points (75 km) apart. Areas within the closed contours are shaded. Note the diagonal symmetry of the f-plane runs and the diagonal asymmetry of the β-plane runs.

in section 3b to derive an estimate for the eddy radii. An alternative form of the momentum balance relation for northward-flowing WBC in a concave solid corner (3) can be derived by noting that, at $x \to \infty$, the zonal flow is geostrophic in the y direction so that (3) can be written as (northward WBC)

$$\int_0^L hv^2\,dx + \frac{g'}{2}\int_0^{L_2}[H_0^2 - h^2(x,0)]\,dx - \beta\iint_S(\psi - \psi_\infty)\,dx\,dy = 0. \quad (8a)$$

It is straightforward to show that, for a southward-flowing WBC,

$$-\int_0^L hv^2\,dx + \frac{g'}{2}\int_0^{L_2}[h^2(x,0) - H_0^2]\,dx - \beta\iint_S(\psi - \psi_\infty)\,dx\,dy = 0. \quad (8b)$$

In the next two sections we shall use (8a) and (8b) to derive analytical expressions for the eddy radius. We shall treat the cases of northward- and southward-flowing WBC separately (because the scales are different).

1) NORTHWARD-FLOWING WBC AND THE ANTICYCLONE

As pointed out earlier, the numerical simulations indicate that the average value of the upper-layer thickness

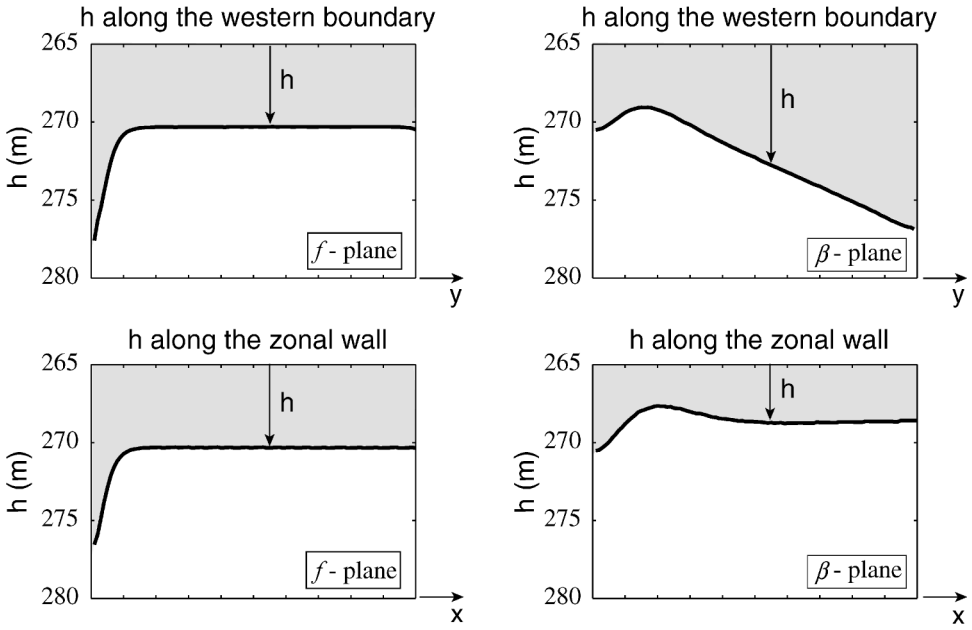

FIG. 8. The f-plane upper-layer thickness h (in m) (upper left) along the western boundary and (lower left) along the zonal wall at day 2500; β-plane upper-layer thickness along (upper right) the western boundary and (lower right) the zonal wall at day 2500. Shaded area is the upper layer. The horizontal axis marks are 10 grid points (75 km) apart.

on the zonal wall is approximately H_0 (the value of h on the zonal wall as $x \to \infty$). Although we cannot come up with any argument explaining why this should be so, we shall use this information for our calculations and neglect the second term in (8a). Recall that, on an f plane, the pressure term is negative and that a neglect of a negative term would overestimate the eddy size. We shall assume here that this is also true on a β plane, implying that our estimate will be a lower bound on the eddy size. With the above neglect, the momentum balance (8a) reduces to

$$\int_0^L hv^2\,dx = \beta \iint_S \hat{\psi}\,dx\,dy, \tag{9}$$

where L is the boundary current width, $\hat{\psi} = \psi - \psi_\infty$, and ψ_∞ is the streamfunction at $x \to \infty$.

Next, we take the following scales:

$$L \sim O(R_d), \qquad \Delta H = (H - H_0) \sim O(H),$$

$$v \sim O[(g'H)^{1/2}],$$

$$\hat{\psi} \sim O\left(\frac{g'H^2}{f_0^2}\right) \quad \text{in the current,} \quad \text{and}$$

$$\hat{\psi} \sim O\left(\frac{g'H_e^2}{f_0^2}\right) \quad \text{in the eddy,}$$

where $R_d = (g'H)^{1/2}/f_0$ and H_e is the thickness scale for the eddy. Note that the second term in (8a) is nonzero only in the eddy and the boundary current (because the streamfunction ψ coincides with ψ_∞ in the interior). Following Nof and Pichevin (1999) we now take $R_{de} = R_d/\varepsilon^{1/6}$ where $\varepsilon \equiv \beta R_d/f_0$ and obtain the leading-order balance,

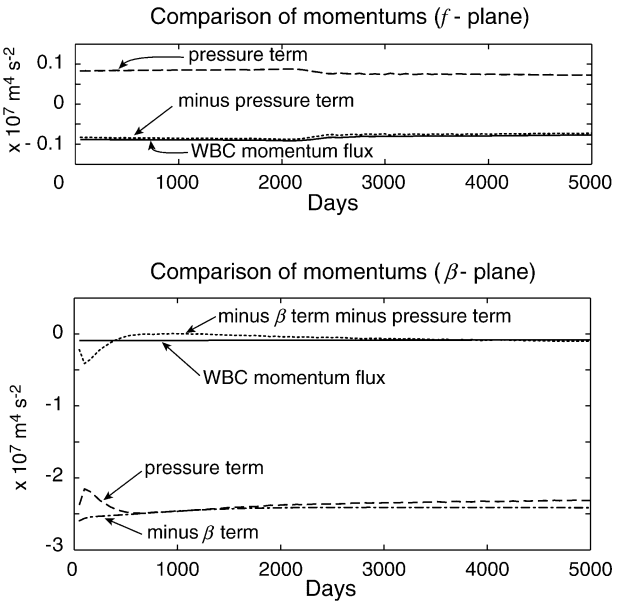

FIG. 9. Terms of the momentum balance (13) computed from the (upper) f-plane expt E2 and the (lower) β-plane expt E4. Note that the f-plane run reaches a steady state right away [within a period of $O(f - 1)$] while the β-plane run takes 500 days to reach a steady state.

$$\int_0^{L^{(0)}} h^{(0)}[v^{(0)}]^2\, dx^* = \iint_{S_e} \psi_e^{(0)}\, dx_e^*\, dy_e^*, \quad (10)$$

where $h^{(0)}$, $v^{(0)}$, $\psi_e^{(0)}$, and $L^{(0)}$ are the zeroth-order approximations of the respective dependent variables.

Next, we take the flow to have zero potential vorticity and find that the solutions are straightforward despite the nonlinearity. Note that, with this assumption, the interior of the basin is motionless (with thickness H) and the velocity is zero along the bounding streamline of the current offshore (see, e.g., Anderson and Moore 1979). As we shall see later, in this limit, the obtained estimate is a lower bound on the eddy radius. The leading-order velocity and thickness for a zero potential vorticity northward-flowing boundary current are

$$v = \begin{cases} f_0(L - x), & x \le L \\ 0, & x > L \quad \text{and} \end{cases} \quad (11)$$

$$h = \begin{cases} H - \dfrac{f_0^2(L - x)^2}{2g'}, & x \le L \\ H, & x > L, \end{cases} \quad (12)$$

where $L = 2^{1/2}R_{de}$ for $R_{de} = [g'(H - H_0)]^{1/2}/f_0$. Since the eddy's upper-layer thickness scale is $H_e = H(R_{de}/R_d)^2 = \varepsilon^{-1/3}H$, we can take $h_e = 0$ along the eddy's boundary and find that, for the zero potential vorticity eddy (i.e., $v_\theta = -f_0 r/2$), (8)–(10) give

$$R_{anti} = 2\left(\frac{2^{3/2}}{\pi}\right)^{1/6}\left(\frac{H - H_0}{H}\right)^{1/2}\left(\frac{H}{H - H_0} - \frac{3}{5}\right)^{1/6}\frac{R_d}{\varepsilon^{1/6}}. \quad (13)$$

This relation is a lower bound because the zero potential vorticity eddy has the strongest nonlinearity (due to the highest steepness) and, consequently, it also has the smallest radius.

To validate (13) we determine analytically the numerical eddy radius using the parameters of the numerical experiment E5 (Table 1), getting $\varepsilon^{1/6} = 0.42$ and $R = 2.84R_d$. Taking the streamline corresponding to the maximum gradient as the eddy boundary (6.5 Sv in Fig. 4) we find that $3.7R_d$ is the average numerical radius between days 1500 and 5000, in very good agreement with the above analytical estimate ($2.84R_d$). In the next section we shall derive the radius estimate for the cyclonic eddy formed by a southward flowing WBC in a concave solid corner on a β plane. We shall see that the scales of the cyclone are quite different from the scale of the anticyclone.

2) SOUTHWARD-FLOWING WBC AND THE CYCLONE

We proceed in a similar fashion to that of the previous section, pointing out that in this case the eddy upper-layer thickness scales with H so that the obtained eddy size scale is $R_d/\varepsilon^{1/2}$ rather than $R_d/\varepsilon^{1/6}$. A zero potential vorticity flow is impossible here and we take the zeroth-order (basic state) boundary current and eddy to have uniform potential vorticity. We shall use the Csanady (1979) solution for uniform potential vorticity cyclonic eddy (Fig. 10). Next, the variables are expanded around the f-plane solution with potential vorticity depth H, and we ultimately find

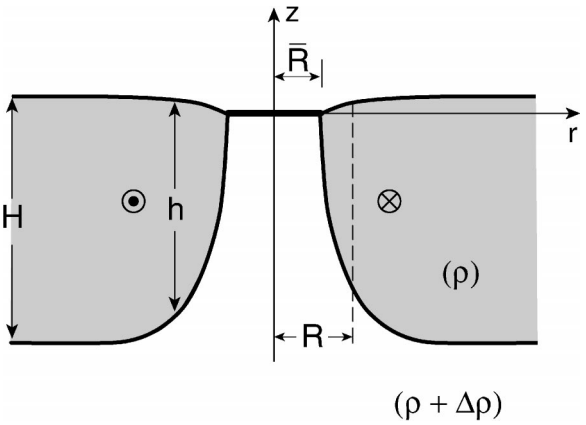

FIG. 10. Schematic representation of our cyclonic eddy; $\overline{R}$ is the radius of the outcropped region, R is the eddy mean radius, and H is the undisturbed thickness at $r \to 0$.

$$R_{cyclone} = \left(\frac{1}{3\pi}\right)^{1/2}\left(\frac{H_0 - H}{H}\right)\left(\frac{H + 2H_0}{H}\right)^{1/2}\frac{R_d}{\varepsilon^{1/2}}. \quad (14)$$

As in the anticyclonic case, (14) is *lower bound* because the uniform potential vorticity eddy outcrops along a contour of radius $\overline{R}$ (where the streamfunction reaches the minimum value of $-g'H^2/f_0$).

Again, to validate (14) we estimate the eddy radius using the parameters of the numerical experiment E6 (Table 1), obtaining $\varepsilon^{1/2} = 0.06$, $R_0 = 1.92R_d$, and $R = 3.35R_d$. As before, taking the streamline corresponding to the maximum gradient as the eddy boundary in E6 (3.5 Sv in Fig. 7), we estimate $4.28R_d$ as the average numerical radius between days 1500 and 5000. This is in fair-to-good agreement with the analytical estimate ($3.35R_d$).

3. The collision problem

In this section we will examine the full collision problem of two opposing WBCs on a β plane (Fig. 11). Recall that, as in the earlier case mentioned above, β is crucial here as, for an analogous f-plane situation, Agra and Nof (1993) showed that net momentum flux of the colliding currents is balanced; that is, no eddies are necessary for the f-plane momentum balance to hold.

a. Formulation

We shall denote the northward-flowing current as the ''main current'' and the southward-flowing one as the ''countercurrent.'' At some point on the western boundary the currents collide and veer offshore as a joined

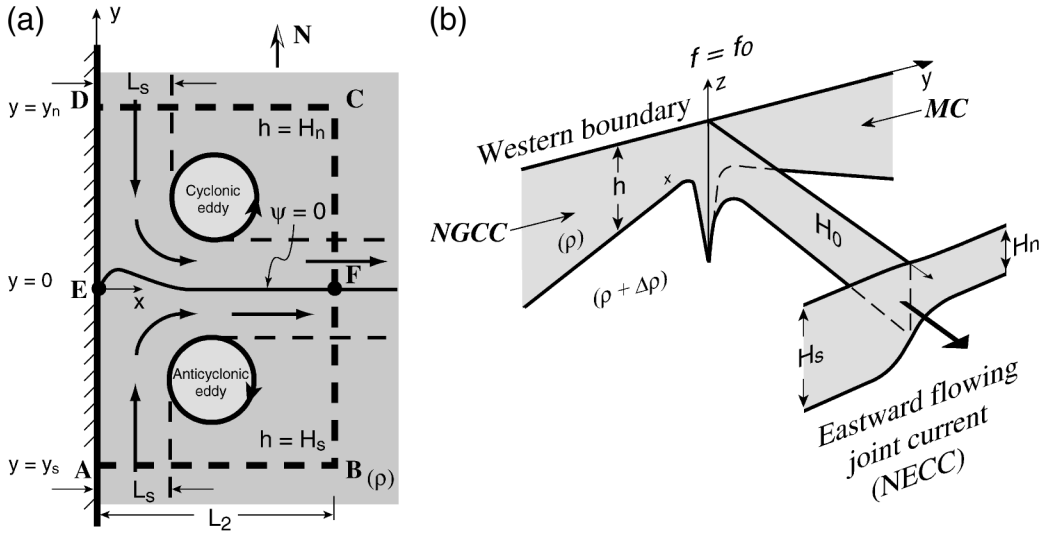

FIG. 11. (a) Schematic top view of the collision of a northward-flowing boundary current (main current) and a southward-flowing boundary current (countercurrent) on a β plane. After the collision the two currents merge into a joined offshore current. East of the western boundary and a few Rossby radii away from the dividing streamline ($y = 0$) the upper-layer thickness is H_s and H_n (where the subscripts s and n denote south and north). (b) A three-dimensional view of the long wall and along-jet thicknesses.

current. We place the origin of our coordinate system at the collision (stagnation) point on the western boundary and assume that, far east of the western boundary and a few Rossby radii away from the dividing streamline, the upper-layer thickness has a value of H_s in the main current (south) side and H_n in the countercurrent (north) side. Assuming a steady state and integrating (after multiplying by h) the steady, inviscid nonlinear y-momentum equation over the fixed region S bounded by ABCDA, we get

$$\underbrace{\int_0^{L_S} hv^2\,dx - \int_0^{L_n} hv^2\,dx}_{\text{net momentum flux}} + \underbrace{\frac{g'}{2}\int_0^{L_2} [h^2(0, y_s) - h^2(0, y_n)]\,dx}_{\text{pressure term}} - \underbrace{\beta \iint_S \psi\,dx\,dy}_{\beta\text{ term}} = 0, \tag{15}$$

where L_s and L_n are the main current and countercurrent widths, S is the integration region bounded by ABCDA (Fig. 11), L_2 is the zonal width of S, and y_s and y_n are the y coordinates of the southern and northern boundaries of S.

To apply our previous analytical approach to the collision problem, we divide the integration region into two subdomains S^+ and S^-, north and south of $\psi = 0$, respectively:

$$\int_0^{L_S} hv^2\,dx + \frac{g'}{2}\int_0^{L_2} [H_0^2 - h^2(0, \phi)]\,dx - \beta \iint_{S^-} (\psi - \psi_\infty)\,dx\,dy = 0 \quad \text{and} \tag{16}$$

$$\int_0^{L_n} hv^2\,dx + \frac{g'}{2}\int_0^{L_2} [h^2(0, \phi) - H_0^2]\,dx - \beta \iint_{S^+} (\psi - \psi_\infty)\,dx\,dy = 0, \tag{17}$$

where H_0 is the upper-layer thickness on $\psi = 0$ as $x \to \infty$ and ψ_∞ (a function of y only) is the limit of ϕ as $x \to \infty$. As expected, the two have a mutual term

$$\frac{g'}{2}\int_0^{L_2} h^2(x, \phi)\,dx,$$

where $y = \phi(x)$ is a Cartesian representation of the curve $\phi = 0$. We shall see in the next section that the second term in (14) and (15) is approximately zero and that, consequently, our solid corner solutions will also be valid here.

b. Numerical simulations

The parameters for the collision experiment E9 on a β plane (Table 1) are identical to those used for experiments E5 and E6 for the concave corner. Figure 12 shows contour plots of the upper-layer thickness and streamfunction for experiment E9 at day 2500. It is evident that an anticyclonic eddy is formed south of the joined offshore current and cyclonic eddy north of it.

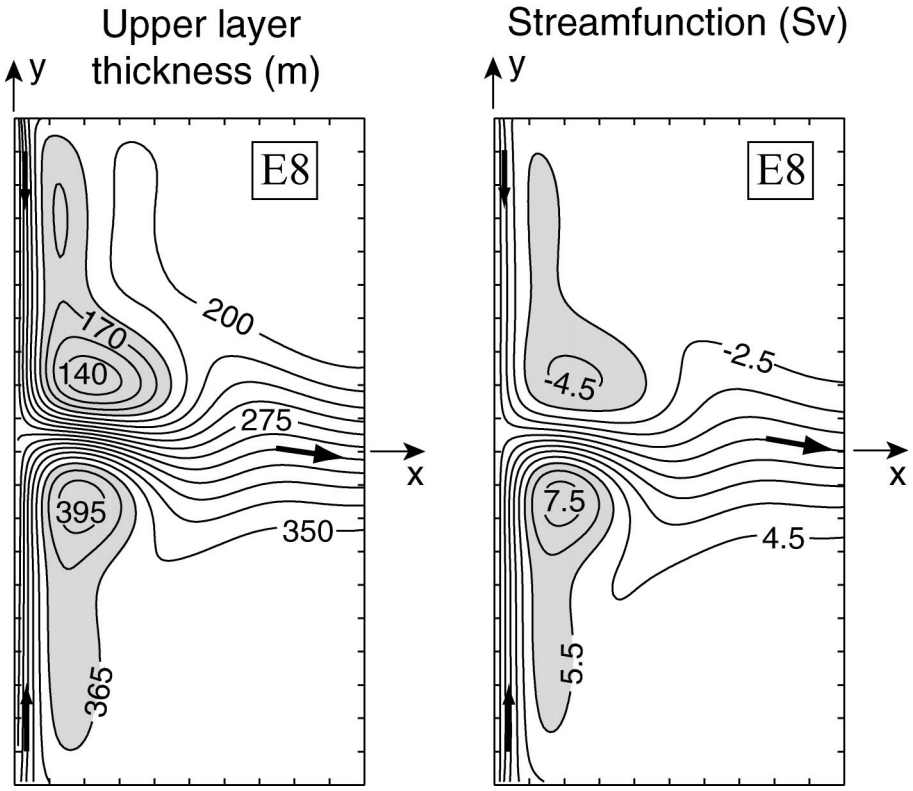

FIG. 12. (left) Upper-layer thickness contours and (right) streamfunction contours for the collision experiment on a β plane at day 2500. The axis marks are 10 grid points (75 km) apart. Areas within closed contours are shaded. Recall that no eddies are produced in the f-plane case (see Fig. 5 in Lebedev and Nof 1997).

Figure 13 shows the upper-layer thickness along the western boundary (upper panel) and along the $\psi = 0$ streamfunction (lower panel). Note the similarity with Figs. 5 and 8 for the β-plane experiments E5 and E6. The pressure force points in the same direction as the momentum flux (in each of the individual subdomains). Therefore, eddies are necessary in order to reach the integrated momentum balances in S^- and S^+ individually. The average value for the upper-layer thickness on the zero streamfunction is 270.8 m while the mean value outside the eddy influence area is 271 m (Fig. 13), showing that, even in the collision problem, the condition that the second term in (16) and (17) vanishes is valid.

Figure 14 shows the numerical estimates for the terms in (15) (upper panel), (16) (middle panel), and (17) (lower panel). In all the cases the inviscid momentum balances hold. The analytical estimates for the flow inside a concave corner can also be used here by considering the $\psi = 0$ streamfunction as a ''wall'' dividing the basin in two parts (the main current side and the countercurrent side). Taking the -4 Sv streamline as the boundary of the cyclonic eddy and the 6.5 Sv streamline as the boundary of the anticyclonic eddy (Fig. 12) we estimate (from the numerics) an average radius of $4.5R_{\rm dn}$ [where $R_{\rm dn} = (g'H_n)^{1/2}/f_0$] and $3R_{\rm ds}$ [where $R_{\rm ds} = (g'H_n)^{1/2}/f_0$]. With differences of less than 26%, we can say that these are in decent agreement with the analytical estimates (of $3.35R_{\rm dn}$ and $2.84R_{\rm ds}$). Recall that these analytical estimates neglect the second terms in (16) and (17).

In the next section we shall apply the theory of the collision of opposing flowing WBC on a β plane to the western equatorial Pacific; in this scenario, the NGCC is the ''main current'' and the MC is the ''countercurrent.''

4. Discussion and summary

The sizes of the eddies as a function of their thickness are shown in Fig. 15. We see that in the linear limit ($H_0/H_n \to 1$ for the cyclone and $H_0/H_s \to 1$ for the anticyclone) both eddies disappear. This is consistent with Morey et al. (1999) who showed that both eddies do not exist in the linear case. Figure 15 also displays the ME and HE radii. We obtained these values by taking 26 Sv for the MC transport and 22 Sv for the NGCC transport. Approximately 11 Sv from the MC and 1 Sv from the SEC flow into the ITF. Using the values calculated by Nof (1996) for the offshore upper layer thicknesses of the colliding currents ($H_n = 97.83$ m for the MC and $H_s = 235.32$ m for the NGCC) we obtain H_0

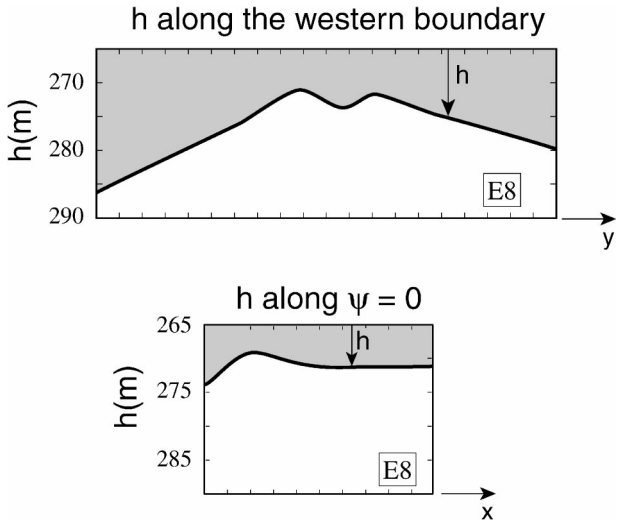

FIG. 13. (upper) Upper-layer thickness h (m) along the western boundary and (lower) along the offshore branch of $y = 0$ for the collision expt E8 at day 2500.

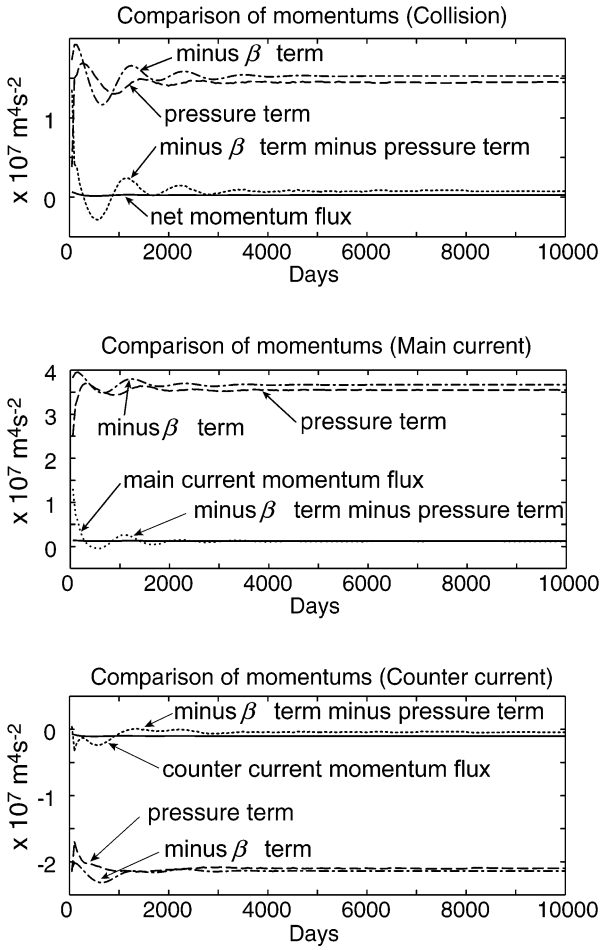

FIG. 14. (upper) Momentum balance for the area containing both colliding currents, (middle) momentum balance for the area south of the zero streamfunction, and (lower) momentum balance for the area north of the zero streamfunction. All terms were computed from expt E8.

$= 170$ m. Substituting the values of H_s, H_n, and H_0 into (11) and (14), we get a radius of $1.144R_{\text{dn}}$ for the Mindanao eddy (where $R_{\text{dn}} = 110$ km and $\varepsilon_n = 0.2$) and a radius of $1.52R_{\text{ds}}$ for the Halmahera eddy (where $R_{\text{ds}} = 171$ km and $\varepsilon_n = 0.3$). The estimated radii compare very well to the observations (Lukas et al. 1991; Kashino et al. 1999) of $1.136R_{\text{dn}}$ (125 km) for the Mindanao eddy and between $1.37R_{\text{ds}}$ and $1.46R_{\text{ds}}$ (between 235 and 250 km) for the Halmahera eddy.

A fundamental question to ask is what causes the factor of 2 or so difference in the calculated eddy sizes. The answer is primarily nonlinearity that manifests itself through both large momentum fluxes and large difference between the thickness north and south of the NECC (H_n and H_s). Variations in the composition of the ITF would, of course, lead to changes in H_0 and, consequently, to variations in the relative sizes of the eddies.

Figures 4 and 8 are the most elucidating of our analysis because they highlight the profound difference between an f-plane and a β-plane flow in a concave solid corner. In the f-plane case there is no eddy and the flow is diagonally symmetric while in the β-plane case there is lack of symmetry and a stationary eddy is attached to the curving flow. The momentum balance relations (4) for nonlinear WBC in the concave solid corner shows that, on an f plane, no eddy is necessary because the pressure force (produced by the difference between the upper-layer thickness) balances the current's momentum flux. On a β plane, on the other hand, the pressure force and the boundary current momentum force point in the same direction. Consequently, a permanent eddy is necessary to produce an opposing β force leading to the required momentum balance. Nonlinearities are of equal fundamental importance because in the linear limit the boundary current momentum flux approaches zero so that no eddy is established. This is why Morey et al.'s (1999) experiments show that there are no eddies when the nonlinearity is very small. In this sense our work has some similarity to the much larger (basin scale) recirculation regions, which also show up only when nonlinearity is present (i.e., they are not present in the limit of a frictional WBC and a Sverdrup interior). The lower bound estimate for the radius of the anticyclonic eddy is given by (13) and, similarly, the lower bound estimate for the radius of the cyclonic eddy is given by (14).

Applying the collision theory for the MC and NGCC in the western equatorial Pacific taking into account only the effective part of each current that participates in the collision process (i.e., excluding the parts that form the ITF), we estimate a diameter of 252 km for the ME and 520 km for the HE. These are in close agreement with the observed values of 250 km and between 470 and 500 km (Lukas et al. 1991; Kashino et al. 1999). We show that the difference between the two is primarily due to nonlinearity (Fig. 15), that is, the stronger mo-

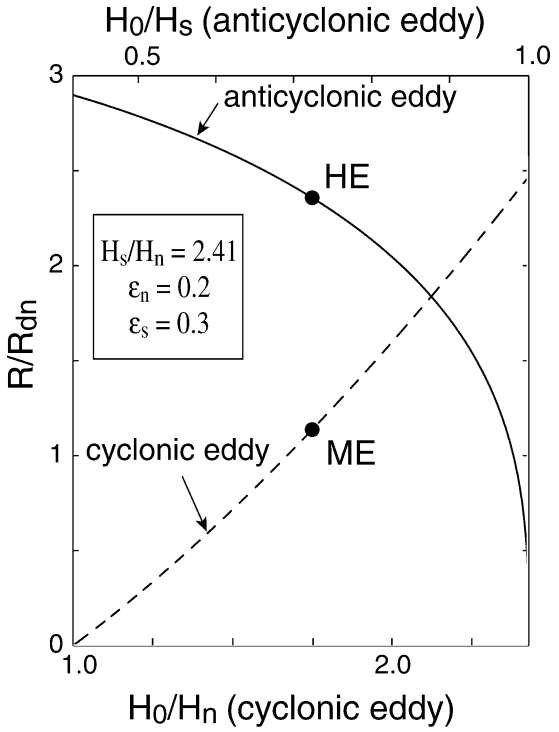

FIG. 15. The eddies' size as a function of the thickness ratio. The importance of nonlinearity is illustrated very vividly here as both the size of the cyclone and the anticyclones go to zero for small amplitude ($H_0/H_n \to 1$; $H_0/H_s \to 1$). Note that, on average, the HE is about 2 times the ME (solid dots). The difference in size is due to the difference in nonlinearity. Note that, for $H_0/H_n > 2$, a larger HE implies a smaller ME and vice versa. Similarly, a weak NGCC (i.e., $H_0/H_s \to 1$) corresponds to no HE but large ME. Likewise, a weak MC (i.e., $H_0/H_n \to 1$) implies a small ME and large HE.

mentum flux of the NGCC relative to that of the MC. This nonlinearity manifests itself in a large difference in the thickness of the upper layer north and south of the NECC. An additional aspect that explains some (~50%) of the difference in the size is the difference in the Coriolis parameter (due to the different latitudes) which contributes to a larger Rossby radius in low latitudes.

Also, note that, according to our solution (Fig. 14), a weaker MC and stronger NGCC (i.e., $H_0/H_n \to 1$) imply smaller ME and larger HE. Similarly, a stronger MC and a weaker NGCC (i.e., $H_0/H_s \to 1$) imply larger ME and smaller HE. This is in agreement with Waworantu (1999) statements that in December–February there is almost no HE but the ME is large (because the NGCC is very weak, i.e., $H_0/H_n \to 1$). In the autumn, on the other hand, the HE is strong and the ME is weak because the NGCC is strong (i.e., H_0/H_n is small). These results are also consistent with the reports of Lukas et al. (1991) and Kashino et al. (2001).

The above arguments show that the physical mechanism proposed here (i.e., that the eddies are necessary to balance the nonlinear momentum flux of their parent currents, the southward-flowing MC and the northward-flowing NGCC) are indeed responsible for the formation of the ME and HE. Of course, our model does not describe all of the oceanic details because it neglects motions below the upper layer as well as the inclination and complexity of the coastline. These could, no doubt, alter our results, but our findings are nevertheless informative because they provide a first glance at the processes in question. We also point out that, although the ITF plays a secondary role in our theory, its existence is essential for the formation of the cross-equatorial flow of the NGCC (see, e.g., Arruda 2002; Nof 1998). Without the ITF there would be no collision and no eddies. Consequently, it is not surprising that variations in the ITF transport lead to variations of the relative sizes of the ME and the HE.

Acknowledgments. This study was supported by the Binational Science Foundation Grant 96-105, National Science Foundation Grants OCE 9911324 and OCE 0241036, National Aeronautics and Space Administration Grants NAG5-7630 and NAG5-10860, and Office of Naval Research Grant N00014-01-0291. Wilton Z. Arruda was funded by ''Conselho Nacional de Desenvolvimento Científico e Tecnológico'' (CNPq-Brazil) under Grant 202436/91-8 and a fellowship from the Inter-American Institute for Global Change Research (IAI) through South Atlantic Climate Change Consortium (SACC). The authors thank Dr. Nobuo Suginohara for his helpful comments and careful reading of the manuscript. We also thank Steve Morey and Jay Shriver for making additional runs of their linear model.

APPENDIX

List of Symbols and Acronyms

B	Bernoulli function, $g'h + (u^2 + v^2)/2$
f	Coriolis parameter ($f_0 + \beta y$)
g'	Reduced gravity, $g\Delta\rho/\rho$
h	Upper-layer thickness
H	Undisturbed interior upper-layer thickness (replaced by either H_n or H_s for the collision problem); see Fig. 2
H_0	Upper-layer thickness on the zonal wall as $x \to \infty$ (Fig. 3)
$\hat{h}$	Upper-layer thickness at the center of the anticyclonic eddy
$H_{\max}$	Upper-layer thickness at the corner (Fig. 3)
H_n, H_s	Upper-layer thicknesses at fixed latitudes in the countercurrent side and main current side (Fig. 11)
L	Boundary current width (Fig. 2)
L_2	Width of square domain S (Fig. 2)
L_n	Countercurrent width (Fig. 11)
L_s	Main current width (Fig. 11)
R	Eddy radius

$\overline{R}$	Radius of the outcropped region in the cyclonic eddy (Fig. 10)
R_d	Rossby radius of deformation, $(g'H)^{1/2}/f_0$
R_{dn}	Rossby radius of deformation, $(g'H_n)^{1/2}/f_0$
R_{ds}	Rossby radius of deformation, $(g'H_s)^{1/2}/f_0$
R_{de}	Rossby deformation radius of the anticyclonic eddy, $(g'H_e)^{1/2}/f_0$
S	Integration area bounded by dashed rectangle in Fig. 2
S^+, S^-	Subsets of S such that $y \geq 0$ and $y \leq 0$, respectively
u, v	Velocity components in Cartesian coordinates
v_θ	Orbital velocity in the eddy
y_s, y_n	Latitudes of the southern and northern boundaries of S (Figs. 2 and 11)
β	Variation of the Coriolis parameter with latitude
ε	Small parameter equal to $\beta R_d/f_0$
ϕ	Cartesian representation of the dividing streamline in the collision problem
ρ, $\Delta\rho$	Density and density difference between the layers
ν	Frictional coefficient
ψ	Streamfunction (defined by $\psi_y = -uh$; $\psi_x = -vh$)
ψ_∞	Limit of ψ as $x \to \infty$
$\hat{\psi}$	$(\psi - \psi_\infty)$
ADCP	Acoustic Doppler current profiler
HE	Halmahera eddy
ITF	Indonesian Throughflow
MC	Mindanao Current
ME	Mindanao eddy
NECC	North Equatorial Counter Current
NGCC	New Guinea Coastal Current
NGCUC	New Guinea Coastal Undercurrent
SEC	South Equatorial Current
WBC	Western boundary current

REFERENCES

Agra, C., and D. Nof, 1993: Collision and separation of boundary currents. *Deep-Sea Res.,* **40A,** 2259–2282.

Anderson, D. L. T., and D. W. Moore, 1979: Cross-equatorial inertial jets with special relevance to very remote forcing of the Somali Current. *Deep-Sea Res.,* **26,** 1–22.

Arakawa, A., 1966: Computational design for long-term numerical integration of the equations of fluid motion: Two-dimensional incompressible flow, Part I. *J. Comput. Phys.,* **1,** 119–143.

Arruda, W., 2002: Eddies along western boundaries. Ph.D. dissertation, The Florida State University, 90 pp.

Bleck, R., and D. Boudra, 1981: Initial testing of a numerical ocean circulation model using a hybrid, quasi-isopycnic vertical coordinate. *J. Phys. Oceanogr.,* **11,** 744–770.

——, and ——, 1986: Wind-driven spin-up in eddy-resolving ocean models formulated in isopycnic and isobaric coordinates. *J. Geophys. Res.,* **91,** 7611–7621.

——, and L. T. Smith, 1990: A wind-driven isopycnic coordinate model of the North and equatorial Atlantic Ocean, 1, Model development and supporting experiments. *J. Geophys. Res.,* **95,** 3273–3285.

Cannon, G. A., 1970: Characteristics of waters east of Mindanao, Philippine Islands, August, 1965. *The Kuroshio, A Symposium on the Japan Current,* J. C. Marr, Ed., East-West Center, 205–211.

Cantos-Figuerola, A., and B. A. Taft, 1983: The South Equatorial Current during 1979–80 Hawaii–Tahiti Shuttle. *Trop. Ocean. Atmos. Newsl.,* **19,** 6–8.

Cessi, P., 1990: Recirculation and separation of boundary currents. *J. Mar. Res.,* **48,** 1–35.

——, 1991: Laminar separation of colliding western boundary currents. *J. Mar. Res.,* **49,** 697–717.

Church, J. A., and F. M. Boland, 1983: A permanent undercurrent adjacent to the Great Barrier Reef. *J. Phys. Oceanogr.,* **13,** 1747–1749.

Csanady, G. T., 1979: The birth and death of a warm-core ring. *J. Geophys. Res.,* **84,** 777–780.

Ffield, A., and A. L. Gordon, 1992: Vertical mixing in the Indonesian thermocline. *J. Phys. Oceanogr.,* **22,** 184–195.

Gordon, A. L., 1986: Inter-ocean exchange of thermocline water. *J. Geophys. Res.,* **91,** 5037–5050.

Gouriou, Y., and J. Toole, 1993: Mean circulation of the upper layers of the Western Equatorial Pacific Ocean. *J. Geophys. Res.,* **98,** 22 495–22 520.

Kashino, Y., H. Watanabe, B. Herunadi, M. Aoyama, and D. Hartoyo, 1999: Current variability at the Pacific entrance of the Indonesian Throughflow. *J. Geophys. Res.,* **104,** 11 021–11 035.

——, E. Firing, P. Hacker, and A. S. Lukiyanto, 2001: Currents in the Celebes and Makulu Seas. *Geophys. Res. Lett.,* **28,** 1263–1266.

Kendall, T. R., 1969: Net transport in the western equatorial Pacific Ocean. *J. Geophys. Res.,* **74,** 1388–1396.

Kessler, W. S., and B. A. Taft, 1987: Dynamic heights and zonal geostrophic transports in the central Pacific during 1979–1984. *J. Phys. Oceanogr.,* **7,** 97–122.

Kundu, P. K., 1990: *Fluid Mechanics.* Academic Press, 638 pp.

Lebedev, I., and D. Nof, 1996: The drifting confluence zone. *J. Phys. Oceanogr.,* **26,** 2429–2448.

——, and ——, 1997: Collision of boundary currents: Beyond a steady state. *Deep-Sea Res.,* **44,** 771–791.

Lukas, R., E. Firing, P. Hacker, P. L. Richardson, C. A. Collins, R. Fine, and R. Gammon, 1991: Observations of the Mindanao Current during the Western Equatorial Pacific Ocean circulation study. *J. Geophys. Res.,* **96,** 7089–7104.

Masuzawa, J., 1968: Second cruise for CSK, Ryofu Maru, January to March 1968. *Oceanogr. Mag.,* **20,** 173–185.

——, 1969: The Mindanao Current. *Bull. Japan Soc. Fish. Oceanogr.,* 99–104.

Morey, S. L., J. F. Shriver, and J. J. O'Brien, 1999: The effects of Halmahera on the Indonesian throughflow. *J. Geophys. Res.,* **104** (C10), 23 281–23 296.

Nof, D., 1996: What controls the origin of the Indonesian throughflow? *J. Geophys. Res.,* **101,** 12 301–12 314.

——, 1998: The ''separation formula'' and its application to the Pacific Ocean. *Deep-Sea Res.,* **45A,** 2011–2033.

——, and T. Pichevin, 1999: The establishment of the Tsugaru and the Alboran gyres. *J. Phys. Oceanogr.,* **29,** 39–54.

Orlanski, I., 1976: A simple boundary condition for unbounded hyperbolic flows. *J. Comput. Phys.,* **21,** 251–269.

Qu, T., H. Mitsudera, and T. Yamagata, 1999: A climatology of the circulation and water mass distribution near the Philippine coast. *J. Phys. Oceanogr.,* **29,** 1488–1505.

Takahashi, T., 1959: Hydrographical researches in the western equatorial Pacific. *Mem. Fac. Fish. Kagoshima Univ.,* **7,** 141–147.

Toole, J. M., E. Zou, and R. C. Millard, 1988: On the circulation of

the upper waters in the western equatorial Pacific Ocean. *Deep-Sea Res.*, **35,** 1451–1482.

——, R. C. Millard, Z. Wang, and S. Pu, 1990: Observations of the Pacific North Equatorial Current bifurcation at the Philippine coast. *J. Phys. Oceanogr.*, **20,** 307–318.

Waworuntu, J., 1999: Water mass transformations and throughflow variability on the Indonesian seas. Ph.D. dissertation, University of Miami, Miami, Florida, 98 pp.

Wyrtki, K., 1956: The subtropical lower water between the Philippines and Iran (New Guinea). *Mar. Res. Indonesia*, **1,** 21–52.

——, 1961: Physical oceanography of the Southeast Asian waters. NAGA Rep. 2, 195 pp.

——, and B. Kilonsky, 1984: Mean water and current structure during Hawaii-to-Tahiti Shuttle Experiment. *J. Phys. Oceanogr.*, **14,** 242–254.